RESEARCH LETTER

Is El Niño *really* changing?

Antonietta Capotondi[1,2] (iD) **and Prashant D. Sardeshmukh[1,2]**

[1]Cooperative Institute for Research in Environmental Sciences, University of Colorado, Boulder, Colorado, USA, [2]Physical Sciences Division, NOAA Earth System Research Laboratory, Boulder, Colorado, USA

Abstract El Niño–Southern Oscillation (ENSO) is the leading mode of tropical Pacific climate variability, with global impacts. Understanding how the statistics of ENSO events may be changing in response to global warming is of great interest and importance for society. A clear detection of such signals in observations has, however, been obscured by large event-to-event differences and apparent "regime shifts" such as that of the late 1970s. In particular, despite extensive research, it is not clear to what extent the observed long-term changes are systemic or random. Here we show using a multicomponent linear inverse modeling technique that statistically significant systemic changes have indeed occurred in ENSO dynamics since the late 1970s and have affected the evolution of El Niño and La Niña events from their embryonic to fully mature stages.

1. Introduction

The behavior of El Niño *apparently* changed in the late 1970s. There were larger year-to-year swings of sea surface temperature (SST) in the eastern equatorial Pacific in the two decades following 1977 than in the two preceding decades (Figure 1), including two especially strong El Niño events in 1982–1983 and 1997–1998 (Figure 2a) and also a hint of a shift toward lower frequencies (Figures 2d and 2e). Such changes led climate scientists to wonder in the early 2000s if the basic character of El Niño was changing [*Fedorov and Philander*, 2000], perhaps as a result of changes in the mean climate associated with global warming. Almost two decades later, the nature of the observed changes in the diversity of El Niño events and regime shifts is still being debated [*Aiken et al.*, 2013; *Aiken et al.*, 2015; *Capotondi et al.*, 2015; *An and Bong*, 2016].

El Niño is a coupled tropical ocean-atmosphere phenomenon involving variations in the upper oceanic heat content, SST, surface winds, and heat fluxes [*McPhaden et al.*, 2006]. The depth and evolution of the thermocline—the interface between the warmer active surface ocean layer and the colder ocean below it—plays a critical role in the development of El Niño events. A deeper than usual thermocline in the eastern Pacific, for instance, is associated with anomalously warm SSTs in that area and a reduced basin-wide east-west SST gradient, which weakens the easterly trade winds. This relaxation of the winds leads to further deepening of the thermocline and additional SST warming, a positive feedback known as the Bjerknes feedback [*Bjerknes*, 1969].

Changes in the background mean state (e.g., mean SST, thermocline depth, and surface winds) can influence the efficiency and timing of such feedbacks, thereby altering the amplitude and frequency of El Niño events [*Fedorov and Philander*, 2000; *Fedorov and Philander*, 2001; *An and Wang*, 2000; *An and Jin*, 2000; *Wang and An*, 2001]. On the other hand, even in a statistically stationary climate, the amplitude, frequency, and triggering of El Niño events are strongly influenced by the amplitude and spatial patterns of the stochastic components of atmospheric forcing. For example, westerly wind bursts over the western and central Pacific can excite eastward propagating oceanic Kelvin waves along the equator that deepen the thermocline in the eastern Pacific and initiate the Bjerknes feedback [*McPhaden*, 1999; *Fedorov*, 2002]. The stochastic atmospheric forcing can also generate lower frequency variations in the ocean due to its larger thermal inertia and hence random decadal modulations in El Niño properties and apparent "regime shifts" [*Wunsch*, 1999; *Wittenberg et al.*, 2014]. And lastly, extratropical influences, in the form of Pacific Meridional Modes [*Chiang and Vimont*, 2004; *Zhang et al.*, 2014] that are themselves excited by higher latitude wind forcing, can energize both interannual and longer term variations in the equatorial Pacific Ocean [*Di Lorenzo et al.*, 2015]. Understanding the relative importance of these mechanisms of decadal variations in El Niño statistics, whether "systemic" (i.e., due to systematic changes in system dynamics and/or in the patterns and amplitudes of the stochastic forcing) or random, is key to the detection and attribution of significant changes in El Niño behavior due to global warming.
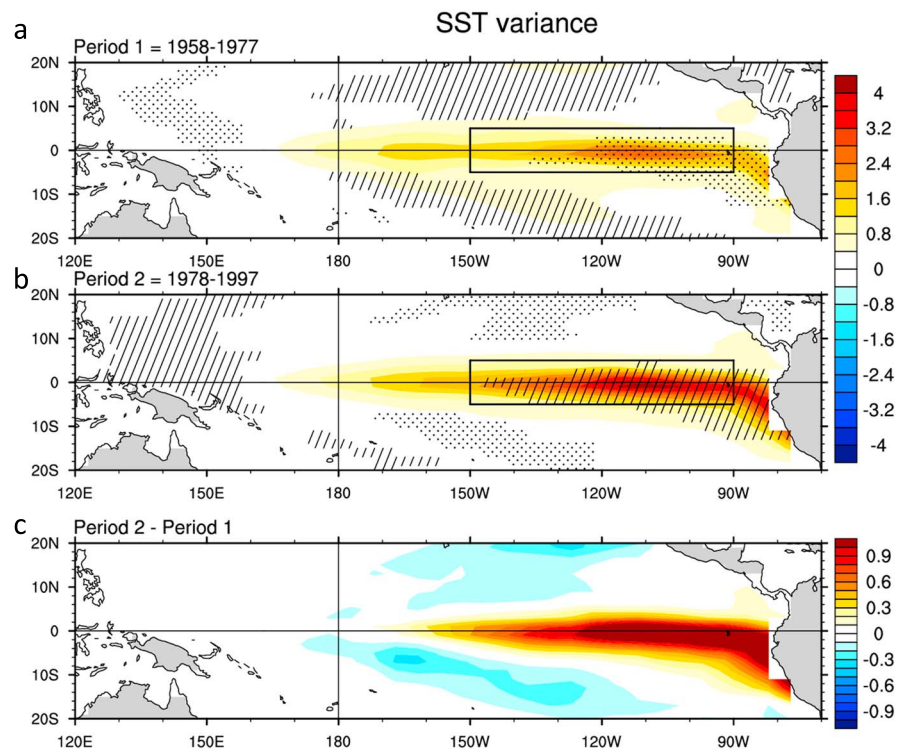
Figure 1. Changes in SST variance. Variance of monthly SST anomalies (°C) in (a) P1 (1958–1977), (b) P2 (1978–1997), and (c) their difference (P2 minus P1). The dotted (hatched) areas indicate P1 variance below (above) the 10th (90th) percentile of the sampling distribution of LIM2 variances centered on the P2 variance (Figure 1a). Similarly, the dotted (hatched) regions indicate P2 variance below (above) the 10th (90th) percentile of the sampling distribution of LIM1 variances centered on the P1 variance (Figure 1b). Both dotted and hatched areas indicate statistically significant differences. The boxes in the top and middle panels show the Niño3 region. Figures S1 and S2 detail how the dotted and hatched areas in Figures 1a and 1b have been determined.

In this paper, we exploit the fact that the evolution of the tropical Pacific Ocean on time scales ranging from a few months to decades can be well described in terms of linearly damped and stochastically forced dynamics [*Penland and Sardeshmukh*, 1995; *Newman et al.*, 2009; *Newman et al.*, 2011], as encapsulated in linear inverse models (LIMs). Informed by the lag-covariances of the observed data, LIMs are able to reproduce El Niño–Southern Oscillation (ENSO) statistics often more successfully than fully coupled climate models [*Newman et al.*, 2009] and can provide us with null hypotheses to assess changes in ENSO characteristics.

2. Data and Methods

The Simple Ocean Data Assimilation (SODA) version 2.0.2 fields, covering the period 1958–2007, were used for this study. The SODA assimilation system uses the Parallel Ocean Program as the ocean model and an optimal interpolation scheme to assimilate all available data from hydrographic stations and expendable bathythermographs [*Carton and Giese*, 2008]. We used the sea surface temperature (SST) and subsurface temperature fields, which, by construction, are dynamically consistent, and chose the depth of the 15°C isotherm (Z15) as a proxy for thermocline depth. To focus on larger scale structures, the SST and Z15 fields were interpolated to 2° latitude × 5° longitude grids.

We represent tropical fields by an anomalous state vector x with SST and thermocline depth (Z15) anomaly components, whose time evolution is governed by a deterministic system feedback matrix L and a stochastic forcing matrix S such that the change Δx over a small time interval Δt is $\Delta x = L\, x\, \Delta t + S\, \Delta w$ (please see supporting information for additional details). The matrix S represents the spatially varying amplitude and coherence structure of the stochastic forcing, and the Δw term represents its random nature as a vector random walk (a Wiener process) over time Δt [*Garcia et al.*, 1987]. Linear inverse modeling involves
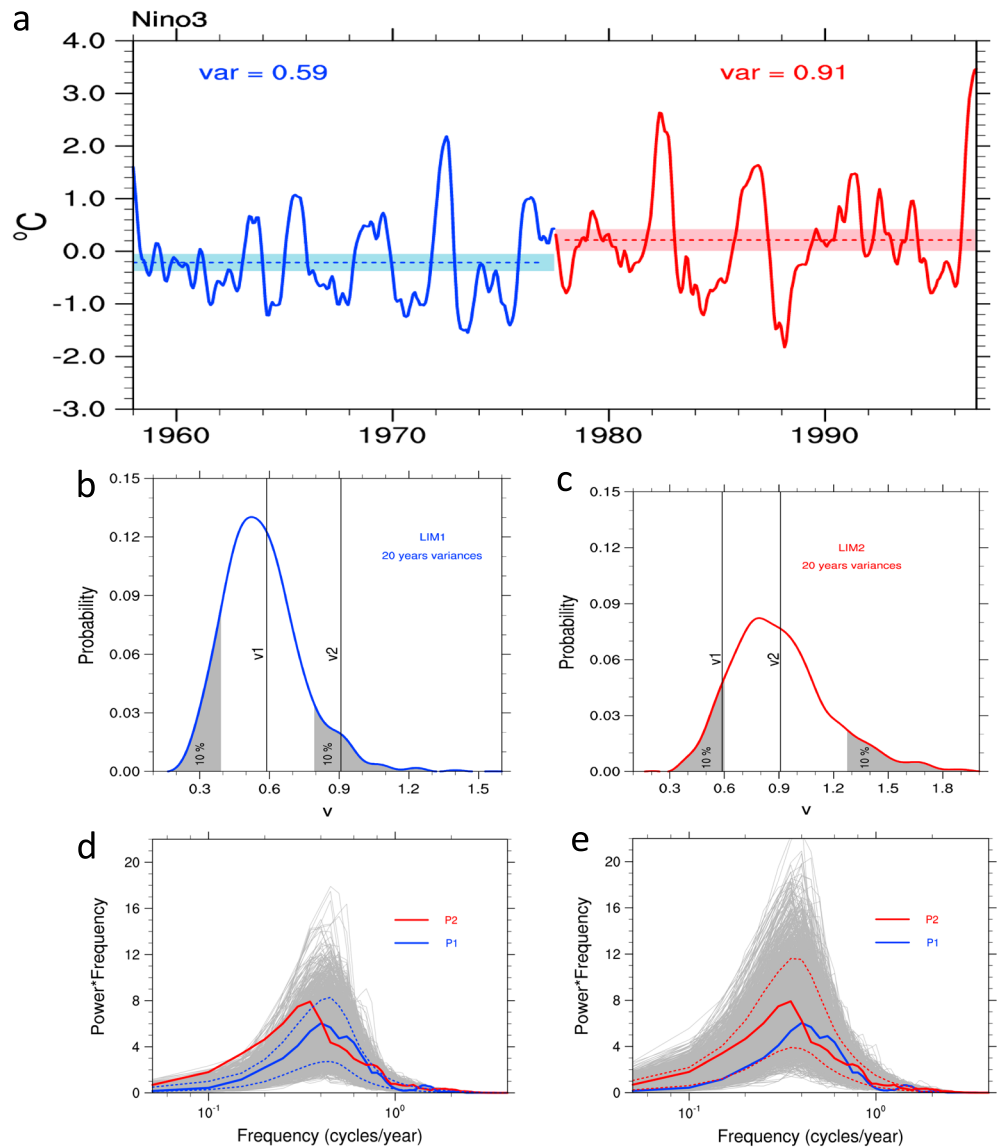
Figure 2. Changes in the statistics of the Niño3 index. (a) Time series of the Niño3 SST index (area averaged monthly SST anomaly in 5°S–5°N, 150°W–90°W, indicated by the box in Figure 1) over 1958–1997. Periods P1 and P2 are highlighted in blue and red, respectively. The dotted blue and red lines indicate the mean value of the Niño3 index over P1 and P2, respectively, while the blue and red shadings indicate the spread in the mean values of the Niño3 index from LIM1 and LIM2. The spread has been computed as twice the standard deviation of the mean values of the index over the 2400 twenty year segments of each LIM simulation. (b) Probability distribution function of the Niño3 variances during P1 from LIM1. (c) Same as Figure 2b, but for P2. The P2 variance ($v_2 = 0.91$) is larger than the 90% percentile of the variance distribution for P1, while the P1 variance ($v_1 = 0.59$) is smaller than the 10% percentile of the variance distribution for P2. (d) Spectra of the Niño3 index over P1 (blue) and P2 (red). The thin gray lines are the spectra of the Niño3 index for each 20 year segment of the LIM1 output. The blue dotted lines indicate the 10th and 90th percentiles of each spectral estimate based on LIM1. (e) Same as Figure 2d, but the thin gray lines are the spectra of the Niño3 index for each 20 year segment of the LIM2 output, and the red dotted lines indicate the 10th and 90th percentiles of each spectral estimate based on LIM2.

estimating **L** and **S** from a time series of **x** [*Penland and Sardeshmukh*, 1995; *Penland*, 1996; *Newman et al.*, 2009; *Newman et al.*, 2011].

We considered two periods, covering the two decades before and after the apparent shift in El Niño behavior in the late 1970s: 1958–1977 (period P1) and 1978–1997 (period P2) and constructed LIMs separately for P1 (LIM1) and P2 (LIM2). To capture the full range of El Niño expressions consistent with the system

dynamics and stochastic forcing observed during P1 and P2, we then ran LIM1 and LIM2 for 48,000 years each, following the procedure outlined in *Penland and Matrosova* [1994], and divided the output into 2400 20 year segments like P1 and P2. All quantities computed for P1 and P2 were then also computed for each of these 2400 20 year segments to estimate their sampling uncertainties associated purely with internal natural variability, that is, with random realizations of Δw. We then asked whether the observed El Niño behavior in P2 was consistent with LIM1 and its associated sampling distribution. Rejecting this null hypothesis would allow us to conclude that the El Niño dynamics in P2 was significantly different from that in P1. Conversely, we also asked whether the observed El Niño behavior in P1 was consistent with LIM2 and its associated sampling distribution. Rejecting this second null hypothesis would allow us to conclude that El Niño dynamics in P1 was also significantly different from that in P2. We considered it important to address both of these questions because rejection of the null hypothesis in one case would not necessarily imply that in the other, especially if the observed variability in the two periods was different. We were thus interested in ascertaining not only to what extent the observed statistics in P2 were inconsistent with the dynamics in P1 but also vice versa.

To assess whether the spatial patterns of the SST and Z15 variances during P1 were significantly different from those in P2, we compared the variance at each location during P1 with the sampling distribution of the variance at the same location obtained from LIM2. Values in the lower and upper 10% percentiles were considered significant. Vice versa, variances during P2 were considered significantly different from those in P1 at those locations where they fell in the lower and upper 10% tails of the LIM1 sampling distribution. This procedure is illustrated in detail in Figures S1 and S2.

3. Results

3.1. Did El Niño Change in the Late 1970s?

The observed variability of monthly SST anomalies was different in P1 and P2 over much of the tropical Pacific domain (Figure 1). The variance at many locations in P2 (Figure 1b) was above the 90th percentile, and at some others below the 10th percentile, of the sampling distribution of variance values estimated from the 2400 20 year segments of the LIM1 run. Such values were considered significantly different from those in P1. Conversely, areas where the variance values in P1 (Figure 1a) were significantly different from those in P2 were similarly identified using the 20 year segments of the LIM2 run. Broad areas of the variance pattern show significant differences between the two periods, including most of the Niño3 region of large SST variability (box in Figures 1a and 1b). This is confirmed by the statistics of the area-averaged SST anomalies in the Niño3 region (Figure 2). The variance v_2 of the Niño3 SSTs in P2 was in the higher tail of the LIM1 sampling distribution centered on v_1 (Figure 2b), and conversely, its variance v_1 in P1 was near the lower tail of the LIM2 sampling distribution centered on v_2 (Figure 2c). Performing a similar analysis of the Niño3 SST spectra for P1 and P2 (Figures 2d and 2e), we find a shift to longer time scales (higher power at lower frequencies) in P2 that is significant relative to the LIM1 sampling distribution of the spectral estimates in P1. Conversely, the low-frequency spectral power in P1 is near the lower tail of the LIM2 sampling distribution of the spectral estimates in P2 (Figure 2e), although only slightly lower than the 10th percentile values at periods longer than ~4 years.

As already mentioned, an important aspect of El Niño evolution is associated with variations in thermocline depth, as reflected in the variability of the depth of the 15°C isotherm (Z15) in our data set. The spatial patterns of the Z15 variance in both periods (Figure 3) show maxima in the far eastern Pacific where the thermocline deepens during warm El Niño events and shoals during cold La Niña events and also in the western Pacific around 6°N and 6°–10°S. These latitudes are near those of the Intertropical Convergence Zone (ITCZ) in the Northern Hemisphere and South Pacific Convergence Zone (SPCZ) in the Southern Hemisphere, whose displacements in response to equatorial warming result in meridional shifts of the trade winds and excitation of westward propagating oceanic Rossby waves [*Capotondi et al.*, 2003]. Interestingly, in contrast to SST, the larger Z15 variance values in P2 in the eastern Pacific are generally not significant. The changes in the western Pacific are, however, significant and likely associated with a more equatorward position of the ITCZ and SPCZ in P2 when stronger El Niño events occurred, and the equatorial Pacific was warmer than average [*Cai et al.*, 2012; *Borlace et al.*, 2014; *An and Bong*, 2016].
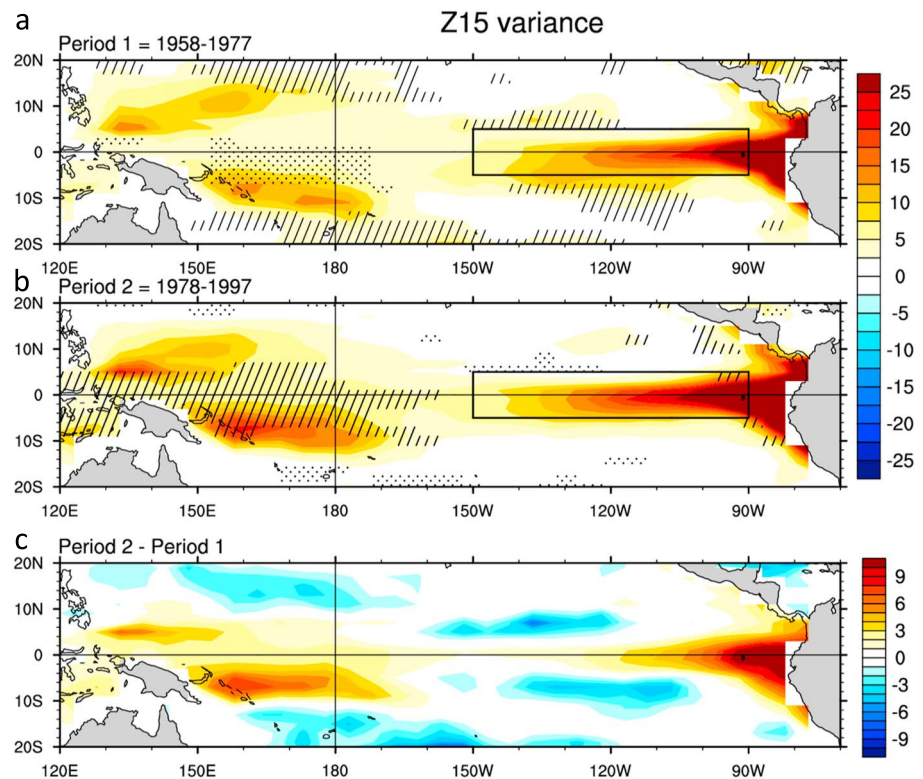
Figure 3. Changes in thermocline depth variance. Same as Figure 1, but for thermocline depth.

### 3.2. Which Part of the El Niño System Changed?

Having identified significant changes in some key aspects of El Niño from P1 to P2, we then used the LIM framework to investigate to what extent these differences were due to changes in the system dynamics or in the amplitude and spatial patterns of the stochastic forcing. One may expect some changes in individual elements of the estimated dynamical feedback and stochastic forcing matrices **L** and **S** to be just due to sampling. Such changes may be locally significant, as in significant reported differences in El Niño propagation characteristics after the late 1970s [*Aiken et al.*, 2013]. However, our main interest was in characterizing and establishing the global significance of changes in **L** and **S** through some overall measure of ENSO dynamics. To this end we exploited the fact that the growth of El Niño events from their embryonic to mature stages can be mathematically characterized as the constructive interference of a subset of dynamical modes, i.e., the eigenvectors of **L**, that are most important in the evolution of ENSO events. Specific combinations of these eigenvectors produce optimal initial conditions for growth over a specified time interval τ, usually 2–3 seasons, to an optimal final state closely resembling a fully developed El Niño state [*Penland and Sardeshmukh*, 1995; *Newman et al.*, 2009; *Newman et al.*, 2011, *Compo and Sardeshmukh*, 2010; *Capotondi and Sardeshmukh*, 2015]. The pair of optimal initial (ϕ_i) and final (ϕ_f) states, which are robust and integral aspects of the **L** operator, thus provide efficient metrics for examining overall changes in ENSO dynamics. The optimal final fields for P1 and P2 (ϕ_f^{P1} and ϕ_f^{P2}; Figures 4b and 4d) calculated using LIM1 and LIM2 both show a fully developed El Niño state, with extensive warming in the central and eastern Pacific, a deeper thermocline in the east, and shallower in the west. However, in P2 the positive SST anomalies are more narrowly confined near the equator in the central and eastern Pacific, and the negative SST anomalies are more extensive in the western northern tropics.

The associated optimal initial fields (Figures 4a and 4c) both show initial warm anomalies extending southwestward from the coast of California to the central-western equatorial Pacific, reminiscent of the North Pacific Meridional Mode [*Chiang and Vimont*, 2004]. Significant differences in the initial fields can be seen along the equator, where the optimal initial pattern ϕ_i^{P2} (Figure 4c) has a large and meridionally narrow positive anomaly, indicative of reduced equatorial upwelling, while ϕ_i^{P1} (Figure 4a) shows weak negative
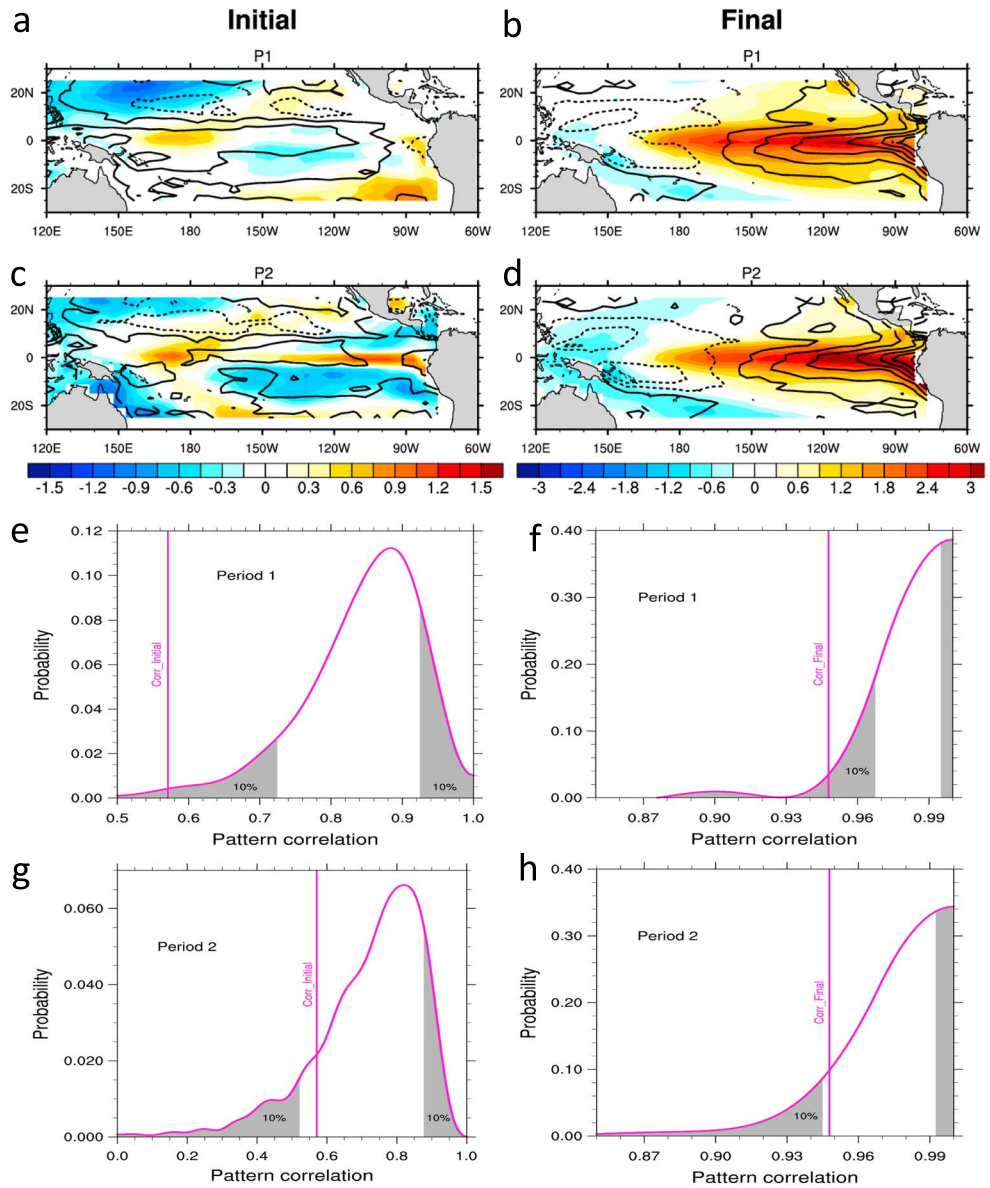
Figure 4. Changes in ENSO dynamics. Initial and final optimal structures of ENSO evolution in (a and b) P1 and (c and d) P2. Shading is for SST, while contours are for thermocline depth, with solid lines indicating positive values and dashed lines indicating negative values. (e–h) Statistical significance of the differences in optimal structures between P1 and P2. The pattern correlation of the optimal initial patterns in P1 and P2 (Corr_Initial = 0.57) is indicated by the magenta line in Figures 4e and 4g, while the pattern correlation of the two optimal final patterns (Corr_Final = 0.948) is the magenta line in Figures 4f and 4h. (e) PDF of the pattern correlations of ϕ_i^{P1} with the optimal initial structures obtained from each of the 2400 20 year segments of the LIM1 run. Figure 4f is the same as Figure 4e, but for the final optimal structures. Figures 4g and 4h are the same as Figures 4e and 4f, but for the pattern correlations of ϕ_i^{P2} and ϕ_f^{P2} with the initial and final patterns, respectively, obtained from each 20 year segment of the LIM2 run.

anomalies in the central part of the basin. The reduced equatorial upwelling during P2 can be expected to be associated with weaker equatorial easterly winds and reduced poleward Ekman transport in the upper ocean, a factor that may explain the cold SST anomalies on either side of the equator, and especially in the southern tropics east of the date line, as seen in Figure 4c. Another notable difference in the initial SST anomaly patterns between P1 and P2 is the warming in the Southeastern Pacific in P1. This SST anomaly pattern, which is similar to the South Pacific Meridional Mode [Zhang et al., 2014], is not seen in P2. The deepening of the thermocline in the optimal initial fields is more confined along the equator in P2 and displays
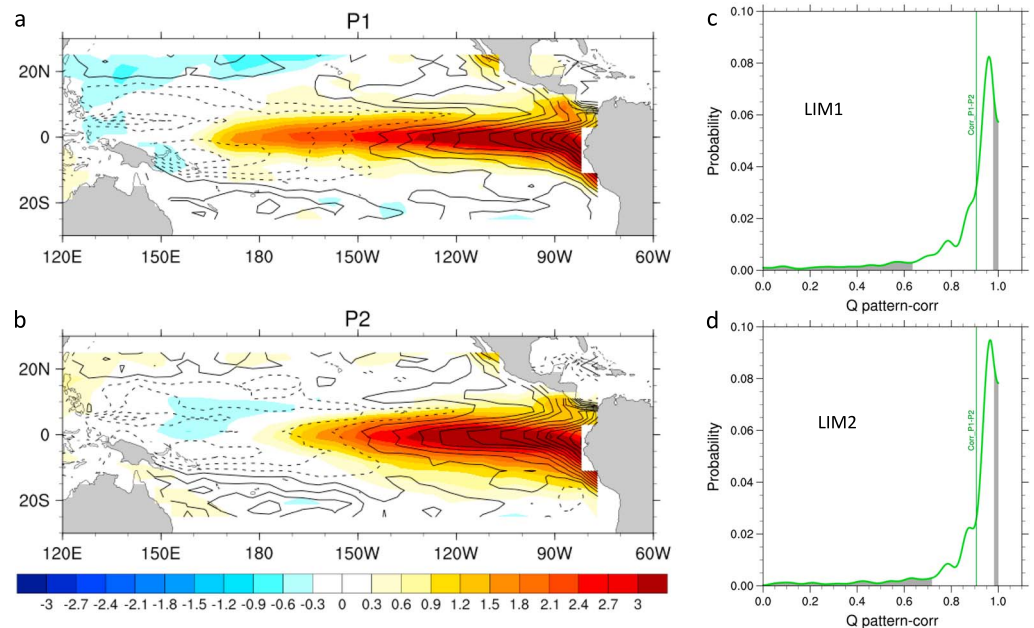
Figure 5. Changes in the stochastic forcing variance. Spatial structure of the leading eigenvector of SS^T for (a) P1 and (b) P2. Shading is for SST, while contours are for thermocline depth (solid contours for positive values and dashed contours for negative values). The pattern correlation between the spatial structures in Figures 5a and 5b is indicated by the vertical green line (Corr_P1-P2) in Figures 5c and 5d. (c) PDF of the pattern correlations between the spatial structure in Figure 5a and the leading eigenvector of SS^T for each of the 2400 20 year segments of LIM1. (d) PDF of the pattern correlations between the spatial structure in Figure 5b and the leading eigenvector of SS^T during each of the 2400 20 year segments of LIM2. Notice that corr_P1-P2 is well within the lower and upper 10% percentiles of both distributions (gray shading), indicating that the leading structures of stochastic forcing in the two periods are not significantly different from each other.

positive anomalies also in the far eastern Pacific, a factor known to be conducive to the development of El Niño events with larger SST anomalies in that area [*Capotondi and Sardeshmukh*, 2015].

Are these optimal patterns for P1 and P2 significantly different? We addressed this question through combined SST and Z15 pattern correlations of the respective fields, comparing the pattern correlations of ϕ_i^{P1} and ϕ_i^{P2} (corr_initial) and ϕ_f^{P1} and ϕ_f^{P2} (corr_final) with the sampling distributions of the pattern correlations obtained from LIM1 and LIM2 (Figures 4e–4h, see supporting information for details). By these measures, the optimal structures in P2 were significantly different from those in P1, indicating that El Niño dynamics changed after the late 1970s.

Did the stochastic forcing matrix **S** also change from P1 to P2? Our metric of choice in this regard is the leading eigenvector of SS^T (where the superscript T denotes transpose; see supporting information), representing the dominant pattern of the stochastic forcing variance. Its pattern (Figure 5) resembles the final El Niño pattern. Although the spatial patterns of the SS^T eigenvectors for the two periods are somewhat different from each other, with the pattern in P2 being meridionally broader and confined east of the date line relative to the pattern in P1, their pattern correlation falls well within the 10% and 90% percentiles of the sampling distributions obtained from LIM1 and LIM2, indicating that a change in this aspect of the system was not responsible for the significant changes in ENSO variability from P1 to P2.

4. Discussion and Conclusions

Our analysis suggests that changes in key El Niño properties observed after the late 1970s, including the variance of surface and subsurface fields and the El Niño spectral characteristics, did not occur "by chance" but were linked to significant changes in the system dynamics as represented in the dominant structures associated with the evolution of El Niño events from their initial to mature stages. What determined these dynamical changes? Some studies have related the changes in ENSO feedbacks to changes in the mean state [*Fedorov and Philander*, 2000; *Wang and An*, 2001; *An and Bong*, 2016]. Indeed, the mean thermocline was

deeper in the eastern and shallower in the western Pacific after the late 1970s, and the surface easterly winds were weaker than in the previous two decades, both factors favoring stronger El Niño variations. But one may wonder what caused those background changes. Due to the amplitude asymmetry between warm and cold (La Niña) ENSO events, with warm events stronger than cold events in the eastern Pacific, epochs with larger ENSO variance, or with a greater number of warm events may be associated with mean conditions that are more "El Niño-like" (larger SST anomalies and deeper thermocline in the eastern Pacific and opposite in the western Pacific), and vice versa for periods with lower ENSO variance or larger number of cold events [*Rodgers et al.*, 2004; *Ogata et al.*, 2013; *Choi et al.*, 2013]. Anthropogenic influences of course cannot be ruled out either.

We note that our results show that while P2 is significantly different from P1, the opposite is not always true. Our interpretation is that the broader range of possible ENSO expressions during P2 is more comprehensive and inclusive of some aspects of P1 than the opposite. This in itself is indicative of significant changes in ENSO behavior. We also acknowledge that our chosen levels for establishing the statistical significance of such changes are not very high. Nonetheless, we believe that our results provide the first objective integrated assessment of ENSO changes over the relatively short (post-1958) recent observational period and outline a suitable methodology for detecting those changes.

It is clear that a fuller understanding of the origin of ENSO diversity and its "regime shifts," whether arising from natural low-frequency variability, climate change, or a combination of both, will require longer observational records of surface and subsurface variables. However, the ability to objectively assess whether a shift in ENSO properties is systemic or random, as presented in this study, is a necessary step toward that understanding.

References

Aiken, C. M., A. Santoso, S. McGregor, and M. H. England (2013), The 1970's shift in ENSO dynamics: A linear inverse modeling perspective, *Geophys. Res. Lett.*, *40*, 1–6, doi:10.1002/grl.50264.

Aiken, C. M., A. Santoso, S. McGregor, and M. H. England (2015), Optimal forcing of ENSO either side of the 1970's climate shift and its implications for predictability, *Clim. Dyn.*, *47*, 967–979.

An, S.-I., and H. Bong (2016), Inter-decadal change in El Niño–Southern Oscillation examined with Bjerknes stability index analysis, *Clim. Dyn.*, *47*, 967–979.

An, S.-I., and F.-F. Jin (2000), An eigen analysis of the Interdecadal changes in the structure and frequency of ENSO mode, *Geophys. Res. Lett.*, *27*, 2573–2576, doi:10.1029/1999GL011090.

An, S.-I., and B. Wang (2000), Interdecadal change of the structure of the ENSO mode and its impact on the ENSO frequency, *J. Clim.*, *13*, 2044–2055.

Bjerknes, J. (1969), Atmospheric teleconnections from the equatorial Pacific, *Mon. Weather Rev.*, *97*, 163–172.

Borlace, S., A. Santoso, W. Cai, and M. Collins (2014), Extreme swings of the South Pacific Convergence Zone and the different types of El Niño events, *Geophys. Res. Lett.*, *41*, 4695–4703, doi:10.1002/2014GL060551.

Cai, W., et al. (2012), More extreme swings of the South Pacific Convergence Zone due to greenhouse warming, *Nature*, *488*, 365–369.

Capotondi, A., and P. D. Sardeshmukh (2015), Optimal precursors of different types of ENSO events, *Geophys. Res. Lett.*, *42*, 9952–9960, doi:10.1002/2015GL066171.

Capotondi, A., M. A. Alexander, and C. Deser (2003), Why are there Rossby wave maxima in the Pacific at 10°S and 13°N?, *J. Phys. Oceanogr.*, *33*, 1549–1563.

Capotondi, A., et al. (2015), Understanding ENSO diversity, *Bull. Am. Meteorol. Soc.*, *96*, 921–938.

Carton, J. A., and B. S. Giese (2008), A reanalysis of ocean climate using Simple Ocean Data Assimilation (SODA), *Mon. Weather Rev.*, *136*, 2999–3017.

Chiang, J. C. H., and D. J. Vimont (2004), Analogous Pacific and Atlantic meridional modes of tropical atmosphere-ocean variability, *J. Clim.*, *17*, 4143–4158.

Choi, K.-Y., G. A. Vecchi, and A. T. Wittenberg (2013), ENSO transition, duration, and amplitude asymmetries: Role of the nonlinear wind stress coupling in a conceptual model, *J. Clim.*, *26*, 9462–9476.

Compo, G. P., and P. D. Sardeshmukh (2010), Removing ENSO-related variations from the climate record, *J. Clim.*, *23*, 1957–1978.

Di Lorenzo, E., G. Liguori, N. Schneider, J. C. Furtado, B. T. Anderson, and M. A. Alexander (2015), ENSO and meridional modes: A null hypothesis for Pacific decadal variability, *Geophys. Res. Lett.*, *42*, 9440–9448, doi:10.1002/2015GL066281.

Fedorov, A. V. (2002), The response of the coupled tropical ocean-atmosphere to westerly wind bursts, *Q. J. R. Meteorol. Soc.*, *128*, 1–23.

Fedorov, A. V., and S. G. Philander (2000), Is El Niño changing?, *Science*, *288*, 1997–2002.

Fedorov, A., and S. G. Philander (2001), A stability analysis of the tropical ocean-atmosphere interactions: Bridging measurements of, and theory for El Niño, *J. Clim.*, *14*, 3086–3101.

Garcia, A. L., M. M. Mansour, G. C. Lie, and E. Clementi (1987), Numerical integration of the fluctuating hydrodynamic equations, *J. Stat. Phys.*, *47*, 209–228.

McPhaden, M. J. (1999), Climate oscillations—Genesis and evolution of the 1997–98 El Niño, *Science*, *283*, 950–954.

McPhaden, M. J., S. E. Zebiak, and M. J. Glantz (2006), ENSO as an intriguing concept in Earth science, *Science*, *314*, 1740–1745.

Newman, M., P. D. Sardeshmukh, and C. Penland (2009), How important is air-sea coupling in ENSO and MJO evolution?, *J. Clim.*, *22*, 2958–2977.

Newman, M., S.-I. Shin, and M. A. Alexander (2011), Natural variation in ENSO flavors, *Geophys. Res. Lett.*, *38*, L14705, doi:10.1029/2011GL047658.

Ogata, T., S.-P. Xie, A. T. Wittenberg, and D.-Z. Sun (2013), Interdecadal amplitude modulation of El Niño-Southern Oscillation and its impacts on tropical Pacific decadal variability, *J. Clim.*, *26*, 7280–7297.

Penland, C. (1996), A stochastic model of Indo-Pacific sea surface temperature anomalies, *Phys. D*, *98*, 534–558.

Penland, C., and L. Matrosova (1994), A balance condition for stochastic numerical models with application to the El Niño–Southern Oscillation, *J. Clim.*, *7*, 1352–1372.

Penland, C., and P. D. Sardeshmukh (1995), The optimal growth of tropical sea surface temperature anomalies, *J. Clim.*, *8*, 1999–2024.

Rodgers, K. B., P. Friederichs, and M. Latif (2004), Tropical Pacific decadal variability and its relation to decadal modulations of ENSO, *J. Clim.*, *17*, 3761–3774.

Wang, B., and S.-I. An (2001), Why the properties of El Nino changed during the late 1970s?, *Geophys. Res. Lett.*, *28*, 3709–3712, doi:10.1029/2001GL012862.

Wittenberg, A. T., A. Rosati, T. L. Delworth, G. A. Vecchi, and F. Zeng (2014), ENSO modulation: Is it decadally predictable?, *J. Clim.*, *27*, 2667–2681.

Wunsch, C. (1999), The interpretation of short climate records, with comments on the North Atlantic and southern oscillations, *Bull. Am. Meteorol. Soc.*, *80*, 245.

Zhang, H., A. Clement, and P. Di Nezio (2014), The South-Pacific meridional mode: A mechanism for ENSO-like variability, *J. Clim.*, *27*, 769–783.